Cell Reports, Volume *26*

Supplemental Information

Widespread Alterations in Translation Elongation in the Brain of Juvenile *Fmr1* Knockout Mice

Sohani Das Sharma, Jordan B. Metz, Hongyu Li, Benjamin D. Hobson, Nicholas Hornstein, David Sulzer, Guomei Tang, and Peter A. Sims

Supplementary Information for "Widespread Alterations in Translation Elongation in the Brain of Juvenile *Fmr1* Knock-Out Mice"

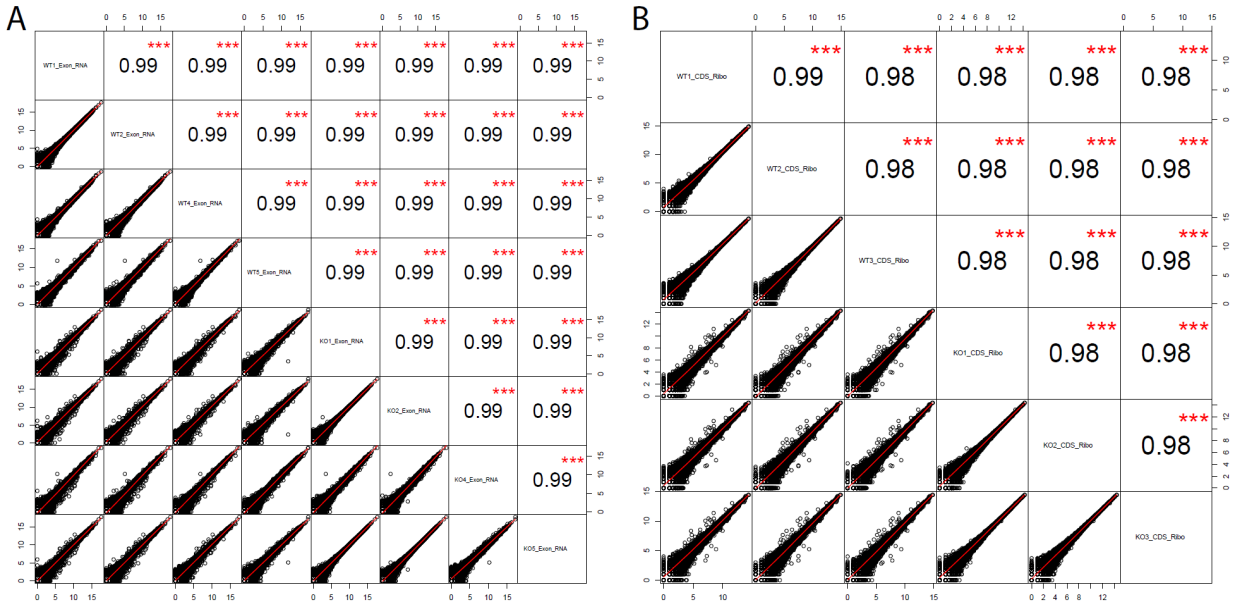

Figure S1. Sample-wise correlation for both RNA-Seq and Ribo-Seq data. Related to Figure 1A-B. A) Pearson correlation coefficient analysis among the all RNA-Seq replicates (A) and Ribo-seq replicates (B). The calculated correlation coefficients in the upper right correspond to the log-log scatter plots comparing gene counts between replicates in the lower left, across the main diagonal. Asterisks indicate $p<0.05$ (*), $p<0.01$ (**), and $p<0.001$ (***).

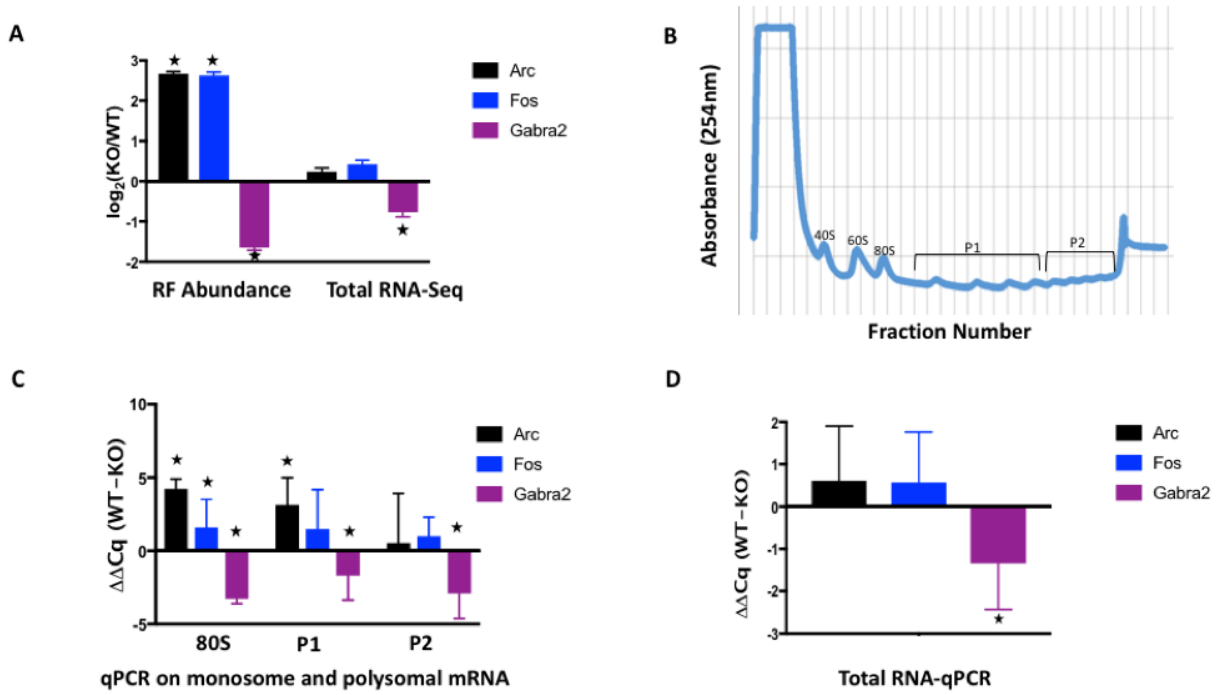

Figure S2. Evaluation of mRNA distribution by polysome fractionation. Related to Figure 1C. A) Bar plots showing differential RF abundance and RNA expression between Fmr1-KO and WT samples for *Arc*, *Fos* and *Gabra2* genes. Differential RF abundance and RNA expression are calculated from Ribo-Seq and RNA-Seq experiments with DESeq2 (Love et al., 2014). Significant changes determined by Benjamini-Hochberg adjusted $p < 0.05$ are designated with asterisks (*). B) Example polysome profile derived from one replicate (KO2). Peaks representing 40S and 60S ribosomal subunits, 80S monosome, and heavier polysomal fractions P1 and P2 are indicated. C,D) Polysome profiling analysis via qPCR of *Arc*, *Fos*, *Gabra2* mRNAs in 80S monosome and polysome fractions (C) and in total RNA (D) between *Fmr1*-KO and WT samples, (n = 3) for each genotype. Levels for each gene are calculated from differences in the cycle count of the gene in question relative to a β-actin control (ΔΔCq) between *Fmr1*-KO and WT samples. Analysis of mRNAs is performed with respective TaqMan probes, data are presented as the average ± standard error of the mean (SEM), and significance determined by Student t-test ($p<0.05$) is indicated with asterisks (*). The error bars represent the SEM. *Arc* and *Fos* are increased while *Gabra2* is decreased in all polysome fractions and total RNA of *Fmr1-KO* relative to WT. *Arc* increase is significant in 80S and P1 fractions, *Fos* increase is significant in 80S, and *Gabra2* decrease is significant across all fractions and in total RNA.

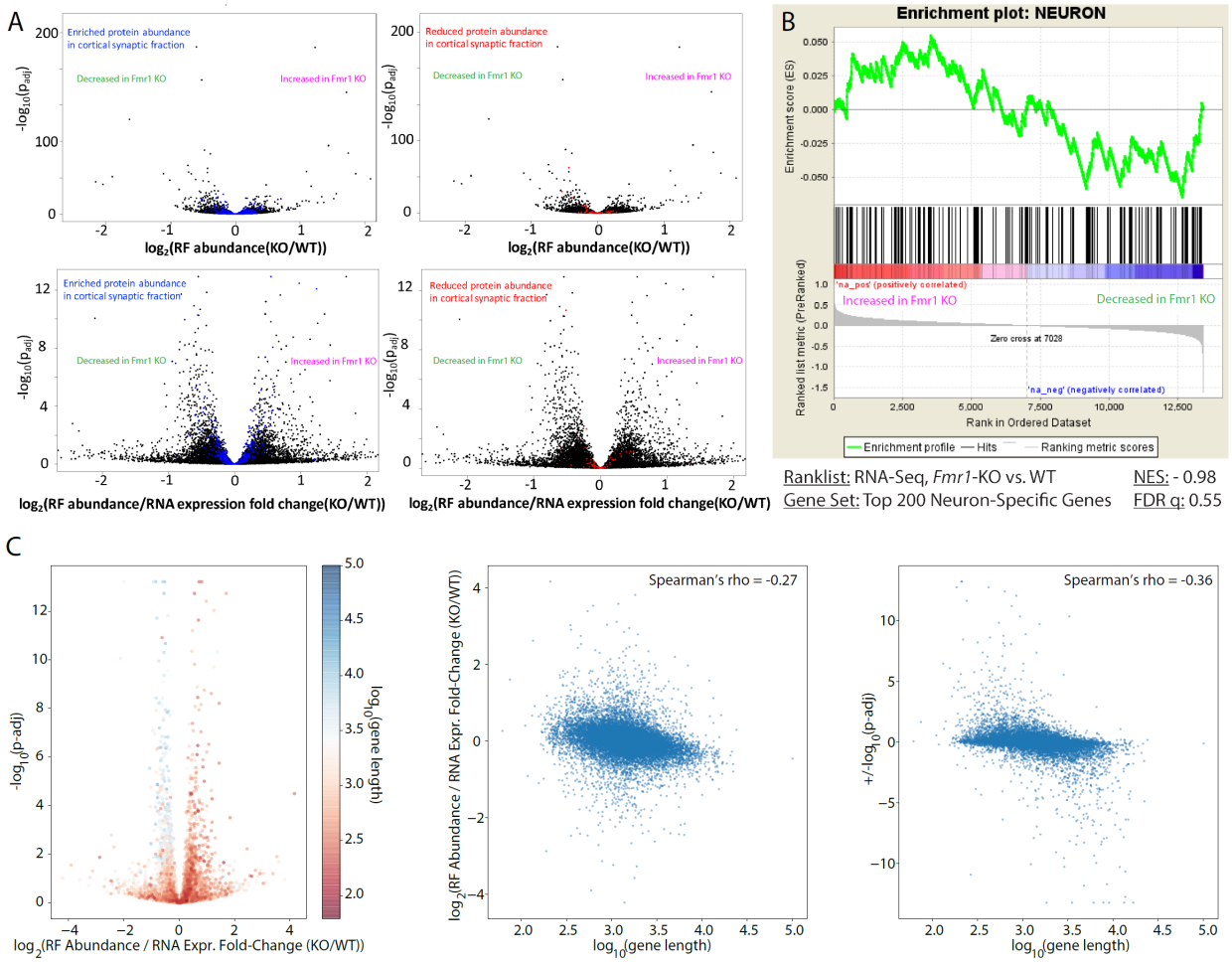

Figure S3. Gene Set Enrichment Analyses (GSEA) of Neuron-Specific genes and proteomically-perturbed gene sets and relationship between coding sequence length and RFApm fold change across genes. **Related to Figure 1 and 2.** A) Volcano plots of the magnitude and significance of change in RF abundance (top two subplots) and RFApm (bottom two subplots) for the genes corresponding to the set of proteins exhibiting increased abundance (in blue, left two subplots) and decreased abundance (in red, right two subplots) in the cortical synaptosomes of P17 Fmr1-KO mice (Tang et al., 2015). Genes of interest are noted in each subplot and colored accordingly. Neither gene set achieved significance of enrichment or depletion in Fmr1-KO vs WT libraries of either datatype (GSEA, FDR q > 0.05; not shown). B) Detailed GSEA enrichment plot and statistics for the top 200 neuron-specific genes (Zhang et al., 2014) in our RNA-seq data, showing no significant enrichment or depletion of this gene set at the transcriptional level in the P24 *Fmr1*-KO mouse cortex (FDR q > 0.05). C) Volcano plot showing the enrichment of longer transcripts among the those with reduced RFApm after *Fmr1* knock-out (left). The two scatter plots (middle and right) show that both the change in RFApm and its significance are anti-correlated with transcript length. These findings are similar to what was reported for *Fmr1* knock-down in Drosophila oocytes(Greenblatt and Spradling, 2018).

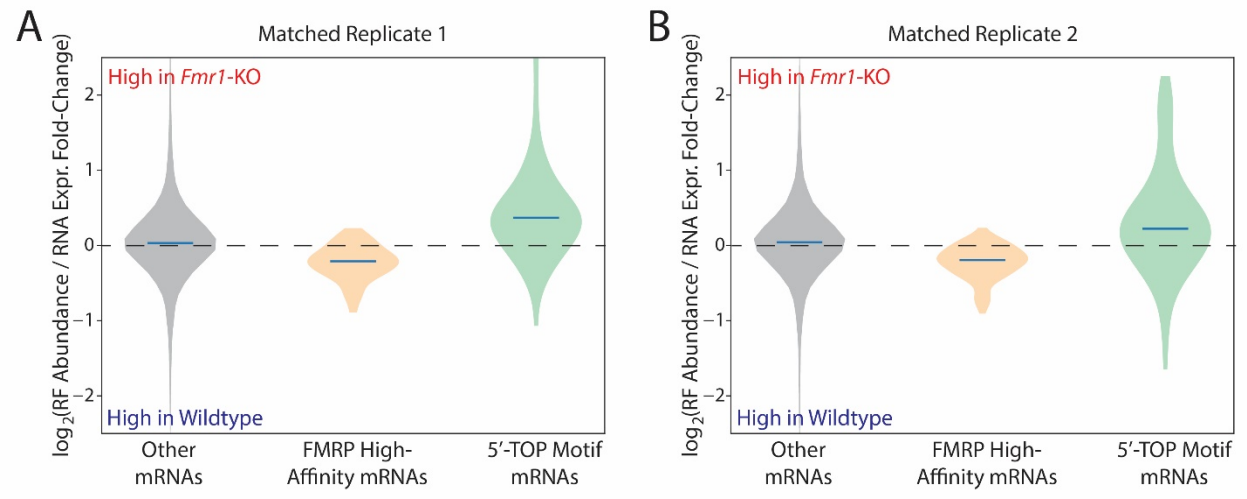

Figure S4. Differential ribosome footprint abundance per mRNA (RFApm) analysis for matched replicates. Related to Figure 2B, 2C. A) and B) are differential RFApm analyses of RNA- and Ribo-seq datasets matched by sample for one *Fmr1*-KO and one WT sample (WT1 vs KO1 and WT2 vs KO2, respectively; see **Table 1**), with y-axis representing log2-fold change in RFApm for these matched data. High-affinity CLIP-seq binding partners for FMRP display a reduction in RFApm, while 5' TOP transcripts exhibit higher RFApm in association with *Fmr1* knockout in both single-replicate analyses, consistent with our main results including all replicates.

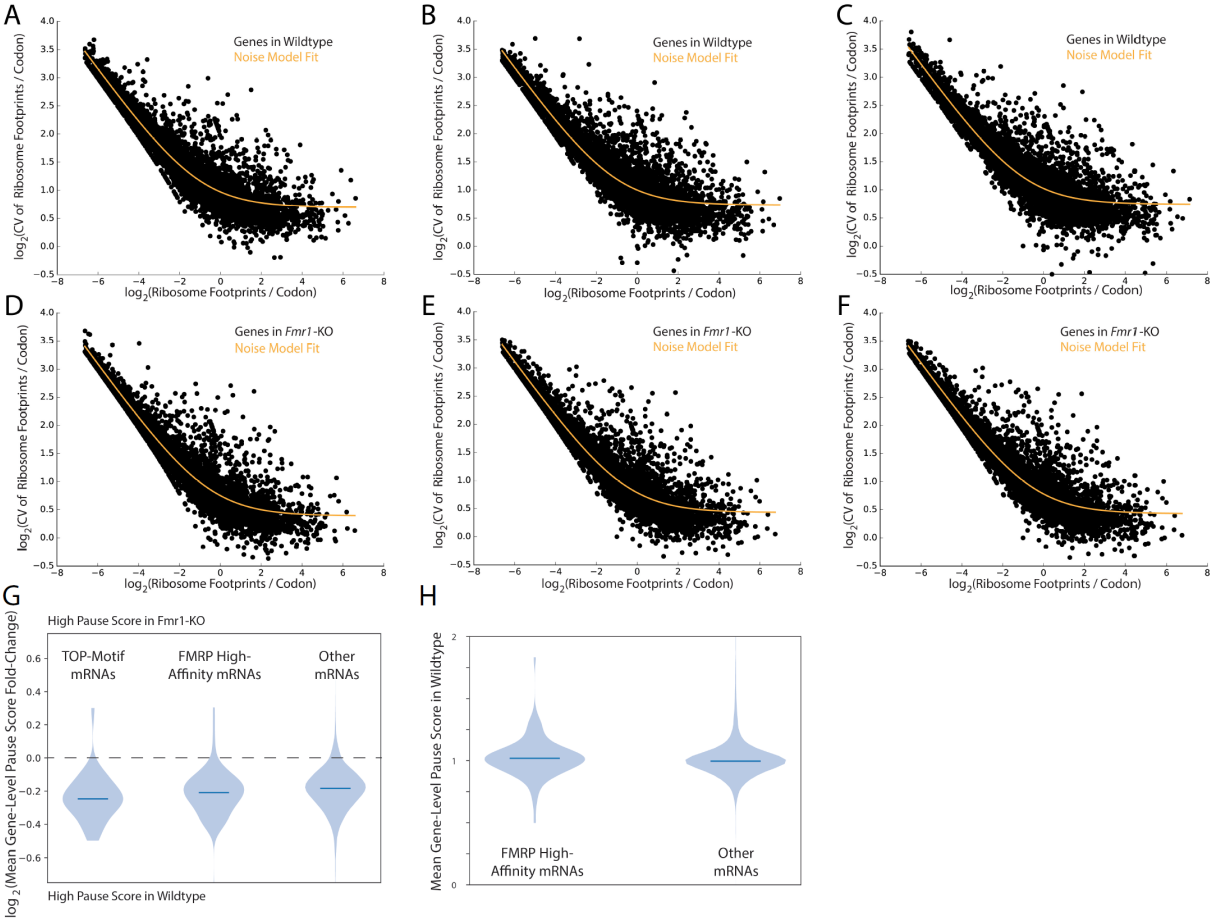

Figure S5. Details of Gene-Level Pausing Analysis. A-F Related to Figure 4A-B; G,H related to Figures 3 and 4.

Coefficient of variation vs. mean of the number of ribosome footprints per codon across all detected genes for individual A-C) wildtype and D-F) *Fmr1*-KO mice with fit to Equation 1. G) Distributions of fold-change of mean gene-level pause scores in TOP motif-containing genes, FMRP high-affinity CLIP-Seq targets, and the transcriptome excluding these sets between WT and *Fmr1*-KO. This analysis reveals decreased pausing in the vast majority of genes in these three sets in *Fmr1*-KO mice and minor differences between their pause score distributions. H) displays gene-level ribosome pausing in both high-affinity CLIP-Seq FMRP binding partners and the remaining mRNAs in the transcriptome in wild-type mice only, demonstrating mildly increased (by ~5%) pausing in the CLIP-Seq targets at baseline. Gene-level pause scores are defined as the coefficient of variation divided by its expectation value from the noise model of the wildtype mouse (from the fit to Equation 1 shown in Figure S5 A-F).